Published in final edited form as:
Cancer Res. 2012 July 1; 72(13): 3405–3413. doi:10.1158/0008-5472.CAN-11-4092.

PTEN and *NF1* inactivation in Schwann cells produces a severe phenotype in the peripheral nervous system that promotes the development and malignant progression of peripheral nerve sheath tumors

Vincent W. Keng[1,2,3,4], **Eric P. Rahrmann**[1,2,3,4], **Adrienne L. Watson**[1,2,3,4], **Barbara R. Tschida**[1,3,4], **Christopher L. Moertel**[4,6], **Walter J. Jessen**[7,9], **Tilat A. Rizvi**[7], **Margaret H. Collins**[8], **Nancy Ratner**[7], and **David A. Largaespada**[1,2,3,4,5]

[1]Masonic Cancer Center, University of Minnesota, Minneapolis, MN 55455, USA

[2]Department of Genetics, Cell Biology and Development, University of Minnesota, Minneapolis, MN 55455, USA

[3]Center for Genome Engineering, University of Minnesota, Minneapolis, MN 55455, USA

[4]Brain Tumor Program, University of Minnesota, Minneapolis, MN 55455, USA

[5]Department of Pediatrics, University of Minnesota, Minneapolis, MN 55455, USA

[6]Department of Pediatric Hematology and Oncology, University of Minnesota, Minneapolis, MN 55455, USA

[7]Division of Experimental Hematology and Cancer Biology, Cincinnati Children's Hospital Research Foundation, Cincinnati Children's Hospital Medical Center, 3333 Burnet Avenue, Cincinnati, OH 45229, USA

[8]Division of Pathology and Laboratory Medicine, Cincinnati Children's Hospital Research Foundation, Cincinnati Children's Hospital Medical Center, 3333 Burnet Avenue, Cincinnati, OH 45229, USA

Abstract

The genetic evolution from a benign neurofibroma to a malignant sarcoma in patients with neurofibromatosis type 1 (NF1) syndrome remains unclear. Schwann cells and/or their precursor cells are believed to be the primary pathogenic cell in neurofibromas because they harbor biallelic *neurofibromin 1* (*NF1*) gene mutations. However, the *phosphatase and tensin homolog* (*Pten*) and *neurofibromatosis 1* (*Nf1*) genes recently were found to be co-mutated in high-grade peripheral nerve sheath tumors (PNSTs) in mice. In this study, we created transgenic mice that lack both *Pten* and *Nf1* in Schwann cells and Schwann cell precursor cells in order to validate the role of these two genes in PNST formation *in vivo*. Haploinsufficiency or complete loss of *Pten* dramatically accelerated neurofibroma development and led to the development of higher-grade PNSTs in the context of *Nf1* loss. *Pten* dosage, together with *Nf1* loss, was sufficient for the progression from low-grade to high-grade PNSTs. Genetic analysis of human sporadic malignant pheripheral nerve sheath tumors (MPNSTs) also revealed down-regulation of *PTEN* expression, suggesting that *Pten*-regulated pathways are major tumor suppressive barriers to neurofibroma progression. Together, our findings establish a novel mouse model that can rapidly recapitulate the onset of human neurofibroma tumorigenesis and the progression to MPNSTs.

Correspondence should be addressed to D.A.L (larga002@umn.edu).
[9]Present address: Biomarker Center of Excellence, Covance, Greenfield, IN 46140, USA.

Keywords

Malignant peripheral nerve sheath tumors; neurofibromatosis type 1 syndrome; neurofibromin 1; neurofibromatosis 1; phosphatase and tensin homolog; desert hedgehog; malignant transformation; Sleeping Beauty transposon system; forward genetic screen; mouse model

Introduction

Neurofibromatosis type 1 (NF1) syndrome is an autosomal dominant inherited disease in which a majority of patients develop benign plexiform and/or dermal neurofibromas. Of great concern is that ~10% of NF1 patients develop malignant peripheral nerve sheath tumors (MPNSTs), which often develop from plexiform neurofibromas and have a poor prognosis (1–3). Schwann cells are believed to be the primary pathogenic cell source in neurofibromas because they show biallelic *neurofibromin 1* (*NF1*) gene mutations (4–6). In addition to *NF1* mutations, MPNSTs harbor many secondary genetic changes and many of these underlying genetic mechanisms are still unknown (7).

Our laboratory and others have successfully demonstrated the effectiveness of the conditional *Sleeping Beauty* (*SB*) transposon system as a forward genetic insertional mutagenesis screen in mice for cancer candidate genes (8–10). Using this *SB* system in a similar forward genetic screen to elucidate candidate genes responsible for sporadic MPNST formation, we directed *SB* insertional mutagenesis specifically in genetically predisposed Schwann cells and were successful in generating many tumors. We identified many candidate mutational drivers of higher-grade peripheral nerve sheath tumors (PNSTs) by identifying commonly mutated genetic loci using the transposon as a molecular tag (*manuscript in preparation*). Importantly, *phosphatase and tensin homolog* (*Pten*) and *neurofibromatosis 1* (*Nf1*) genes were amongst the many candidate genes identified in this screen that tended to be co-mutated in the same high-grade PNSTs ($P < 7.94e\text{-}5$). Inactivation of the *Nf1* gene by the *desert hedgehog* (*Dhh*) promoter driving Cre recombinsase (*Dhh*-Cre) at embryonic age 12.5 elicits plexiform neurofibromas, dermal neurofibromas and abnormal hyper-pigmentation (11). *PTEN*, a negative regulator of the *PI3K/AKT/mTOR* pathway involved in regulation of cell growth and survival, is the most frequently inactivated tumor suppressor gene in sporadic cancer (12). *Pten* dosage is essential for neurofibroma development and malignant transformation in the context of *Kras* activation (13). However, the relationship between *Pten* and *Nf1* in Schwann cell neurofibroma development and its progression to aggressive genetically engineered mouse model-PNST has not been elucidated. In order to further understand the underlying genetic complexity of plexiform neurofibroma and MPNST development, we hypothesized that somatic *Nf1* and *Pten* inactivation in Schwann cells and/or their precursors will promote progressive low-grade and/or high-grade PNST formation. *Dhh*-Cre was used to elicit recombination of $Nf1^{flox/flox}$ (14) and $Pten^{flox/flox}$ (15) alleles, allowing for inactivation of both *Nf1* and *Pten* genes in Schwann cells and/or their precursors. Knowing that *Dhh*-Cre; $Nf1^{flox/flox}$ ($\Delta Nf1$) animals develop low-grade PNSTs, we hypothesized that triple transgenic mice *Dhh*-Cre; $Nf1^{flox/flox}$; $Pten^{flox/flox}$ ($\Delta Nf1/\Delta Pten$) could develop low-grade tumors that would further progress to high-grade PNSTs.

In the current study, our data strongly implicates the synergistic role of *Pten* inactivation to plexiform neurofibroma tumorigenesis and progression to high-grade PNSTs in the context of *Nf1* loss in Schwann cells and/or their precursor cells. Importantly, expression microarray analyses of bulk tumor and cell lines from human NF1 patients also show a selective pressure towards loss of *PTEN* expression during disease progression from a benign neurofibroma to a malignant tumor. This novel mouse model can be used to rapidly model

the onset of low-grade PNST development and its progression to high-grade PNSTs. In addition, this model can be used to test a variety of pharmaceutical agents *in vivo*.

Materials and Methods

Generation of transgenic animals

Generation of transgenic mice carrying the *Dhh* gene regulatory element driving Cre recombinase (*Dhh*-Cre) has been previously described (16) (Supplementary Fig. 1). Transgenic mice carrying the floxed *Nf1* allele that has the essential exons 31 and 32 of the *Nf1* gene floxed with loxP sites has been previously described (14) (Supplementary Fig. 1). The floxed *Pten* allele consists of the essential exons 4 and 5 of the *Pten* gene floxed with loxP sites has been previously described (15) (Supplementary Fig. 1). These singly transgenic mice were crossed to obtain triple transgenic mice containing one allele of each transgene. These triple transgenic mice were then interbred to obtain various experimental and control cohorts (Fig. 1A). Animals were sacrificed when moribund due to paralysis and necropsy performed. All animal work was conducted according to the University of Minnesota's approved animal welfare protocol.

PCR genotyping

Identification of the various genotypes from both adult transgenic animal and pups were performed as follows: Firstly, genomic DNA was isolated from tail clippings using standard proteinase K treatment, phenol-chloroform extraction and ethanol precipitation. Genomic DNA was then dissolved in sterile TE [10mM tris-HCl (pH7.5), 1mM EDTA (pH 8)] and quantified using a Nanodrop spectrophotometer. PCR genotyping was performed using 50 ng of diluted genomic DNA as template in a 25 μl PCR reaction volume. PCR primers used for *Dhh*-Cre were forward 5′-CTGGCCTGGTCTGGACACAGTGCCC′-3′ and reverse 5′-CAGGGTCCGCTCGGGCATAC-3′ (amplicon 385 bp); *Nf1* floxed allele were wild-type (WT) forward 5′-CTTCAGACTGATTGTTGTAACTGA-3′, WT reverse 5′-ACCTCTCTAGCCTCAGGAATGA-3′ and floxed reverse 5′-TGATTCCCACTTTGTGGTTCTAAG-3′ (WT amplicon 480 bp and floxed allele amplicon 350 bp); *Pten* floxed allele were forward 5′-AAAAGTTCCCCTGCTGATTTGT-3′ and reverse 5′-TGTTTTTGACCAATTAAAGTAGGCTGT-3′ (WT amplicon 310 bp and floxed allele amplicon 435 bp). PCR conditions for ReddyMix (Thermo Scientific) were used according to the manufacturer's instructions with an initial denaturing step of 95°C for 2 min; 30- or 35-cycles of denaturing at 95°C for 25 sec, annealing at 55°C for 35 sec and extension at 72°C for 65 sec; followed by a final extension at 72°C for 5 min. PCR products were separated on a 2% agarose gel and genotype determined by the absence or presence of expected amplicons.

Peripheral nerve tumor analysis

PNSTs were carefully removed from the sacrificed animal under a dissecting microscope (Leica), washed and placed in cold phosphate buffered saline (PBS). Any abnormal sciatic nerves, brachial plexi and/or sacral plexi were also removed when necessary. Trigeminal nerves attached to the brain were also observed for any abnormalities. The number of enlarged dorsal root ganglia was counted for the whole spinal cord. All reasonably sized tumor nodules (>2 mm in diameter) were carefully removed from the spinal cord using fine forceps and placed in fresh cold PBS.

Hematoxylin-eosin (HE) staining

Sections for histology were only taken from larger tumor nodules (>2 mm in diameter). Tissues were fixed in 10% formalin, routinely processed and embedded in paraffin. Sections

for histology were cut at 5 microns from the paraffin blocks using a standard microtome (Leica), mounted and heat-fixed onto glass slides. Slides were either stained with HE using standard protocols, or used for immunofluorescence, immunohistochemistry and/or toluidine blue staining as described in the next section.

Immunohistochemistry (IHC), toluidine blue (TB) and immunofluorescence (IF) staining

Formalin fixed-paraffin embedded sections from various tissues were sectioned at 5 microns, mounted and heat-fixed onto glass slides to be used for IHC analyses. Briefly, the glass section slides were dewaxed and rehydrated through a gradual decrease in ethanol concentration. The antigen epitopes on the tissue sections were then unmasked using a commercially available unmasking solution (Vector Laboratories) according to the manufacturer's instructions. The tissue section slides were then treated with 3% hydrogen peroxide to remove any endogenous peroxidases. Blocking was performed at 4°C using a M.O.M. mouse immunoglobulin-blocking reagent (Vector Laboratories) or in appropriate normal serum from the host of the secondary antibody (5% serum in PBS) in a humidified chamber for several hours. For IHC and/or IF, sections were then incubated overnight at 4°C in a humidified chamber using various primary antibodies at the indicated dilutions: Ki67 (1:200) (Novocastra), S100β (1:100) (Santa Cruz), Pten (1:200) (Cell Signaling), phospho-Erk1/2 (1:400) (Cell Signaling), phospho-Akt (Ser473) (D9E) (1:250) (Cell Signaling), Olig2 (1:200) (Abcam) and phospho-S6 (Ser240/244) (1:200) (Cell Signaling). After primary incubation, sections were washed thoroughly in PBS before incubating with horseradish peroxidase-secondary antibody raised against the primary antibody initially used. After thorough washes with PBS, the sections were treated with freshly prepared DAB substrate (Vector Laboratories) and allowed for adequate signal to develop before stopping the reaction in water. Finally, sections were then lightly counter-stained with hematoxylin, dehydrated through gradual increase in ethanol concentration, cleared in Citrosol and mounted in Permount (Fisher).

TB staining for mast cells were performed using standard protocols: Briefly, sections were dewaxed and rehydrated to water, stained with toluidine blue working solution (0.1% toluidine blue O in 0.9% sodium chloride pH 2.3) for 2–3 min, washed 3-times with distilled water before dehydrating quickly through a series of alcohols, clearing in Citrosol and finally mounted in Permount.

IF was performed on formalin fixed-paraffin embedded sections using standard techniques. Briefly, sections were processed as described previously for IHC up to the primary antibody incubation step. Sections were then incubated in fluorochrome-conjugated secondary antibodies (Invitrogen) before mounting in Prolong Gold Antifade Reagent (Invitrogen). Sections were examined using appropriate excitation wavelength.

Histologic evaluation

Sections stained with HE; antibodies to Ki67 and S100β antigens; and with toluidine blue were evaluated for all tumors (17). Each sample was graded using established criteria for tumors arising in genetically engineered mice (18, 19). Briefly, low-grade PNSTs exhibited low cellularity with little if any nuclear atypia and mitotic activity. High-grade PNSTs were increasingly cellular with increasing nuclear atypia and increasing mitotic activity.

Microarray gene expression

Microarray gene expression analysis was performed on purified human Schwann cells taken from normal sciatic nerve, dermal and plexiform neurofibromas and MPNST cell lines as previously described (20, 21). Microarray gene expression analysis was also performed on normal sciatic nerve tissue, dermal neurofibroma, plexiform neurofibroma and malignant

peripheral nerve sheath solid tumor samples obtained from NF1 patients as previously described (20, 21).

Comparison of mouse model with human NF1 patients

Magnetic resonance imaging (MRI) images of different neurofibromas were taken from NF1 patients at the University of Minnesota (IRB study number 1103E97613).

Results

Early postnatal lethality results from Nf1 and Pten inactivation in Schwann cells and/or their precursor cells

Transgenes used to generate the peripheral nerve tumor progression mouse model are shown in Supplementary Figure 1. Transgenic mice carrying all 3 transgenes (*Dhh*-Cre; $Nf1^{flox/+}$; $Pten^{flox/+}$) (*Nf1-het*/*Pten-het*) were interbred to generate both experimental and control cohorts (Fig. 1A). Significant differences in survival rate were observed between: (i) *Dhh*-Cre; $Nf1^{flox/flox}$; $Pten^{flox/flox}$ (Δ*Nf1*/Δ*Pten*) and *Dhh*-Cre; $Nf1^{flox/flox}$; $Pten^{flox/+}$ (Δ*Nf1*/*Pten-het*) ($P < 0.0001$, log-rank test) and (ii) Δ*Nf1*/*Pten-het* compared with *Dhh*-Cre; $Nf1^{flox/flox}$ (Δ*Nf1*) ($P = 0.0006$, log-rank test), indicating *Pten* dosage in the context of *Nf1* inactivation plays an important role for disease progression (Fig. 1B).

In addition, significant differences in survival rate were also observed between: (i) Δ*Nf1*/Δ*Pten* and *Dhh*-Cre; $Nf1^{flox/+}$; $Pten^{flox/flox}$ (*Nf1-het*/Δ*Pten*) ($P < 0.0001$, log-rank test) and (ii) Δ*Nf1*/Δ*Pten* and *Dhh*-Cre; $Pten^{flox/flox}$ (Δ*Pten*) ($P = 0.0001$, log-rank test) (Fig. 1B). Complete inactivation of *Pten* in Schwann cells and/or their precursor cells alone can also contribute to enlarged dorsal root ganglia but at a lower penetrance (Supplementary Fig. 2). Although there was a statistical difference in the survival rate between Δ*Pten* and *Nf1-het*/Δ*Pten* cohorts ($P = 0.0419$, log-rank test), the occurrence of various peripheral nervous system phenotypes was comparable (Table 1). The median survival age for experimental and control cohorts are shown in Table 1. Experimental and control mice became moribund due to paralysis as the result of various peripheral nervous system tumor burden. In contrast, *Nf1-het*/*Pten-het* control mice ($n = 8$) displayed no obvious phenotype and were viable up to >365-days. Several *Nf1-het*/*Pten-het* control mice were sacrificed at various ages (from 189- to 506-days) and all peripheral nerves were normal (Supplementary Fig. 2).

There was also no statistically significant difference in survival rate between experimental cohorts Δ*Nf1*/*Pten-het* and *Nf1-het*/Δ*Pten* ($P = 0.7911$, log-rank test). Others and we have shown that Δ*Nf1* mice have a median survival age of about 243-days ($n = 11$) (11). There was no statistical difference in the survival rate between Δ*Pten* and Δ*Nf1* ($P = 0.3660$, log-rank test), indicating that loss of either tumor suppressor gene can promote Schwann cell tumorigenesis. Biallelic inactivation of *Nf1* and *Pten* in Schwann cells led to rapid postnatal death, resulting in a median survival age of 15-days (Fig. 1B). Increasing levels of *Pten* partially alleviated the severe phenotype, leading to an increase in survival (Fig. 1B). Complete *Nf1* loss is essential for the rapid severe peripheral nervous system phenotype in the context of *Pten* inactivation in Schwann cells and/or their precursor cells (Fig. 1B).

Severe peripheral nervous system phenotype observed in ΔNf1/ΔPten animals

Δ*Nf1*/Δ*Pten* experimental animals displayed a severe early peripheral nervous system phenotype that included enlarged brachial plexi, multiple enlarged dorsal root ganglia and enlarged trigeminal nerves (Fig. 2A, *left*). In contrast, Δ*Nf1*/*Pten-het* animals displayed a similar peripheral nervous system phenotype including enlarged brachial plexi, several large dorsal root ganglia and enlarged trigeminal nerves but at a delayed latency (median age of 172-days) and at a significantly reduced tumor multiplicity (Fig. 2A, **middle and** Fig. 2B).

Δ*Nf1* animals displayed a similar peripheral nervous system phenotype and at a similar tumor multiplicity but with a more delayed latency (median age of 243-days) compared with Δ*Nf1*/*Pten-het* animals (Fig. 2A, *right*). Both Δ*Nf1*/*Pten-het* and Δ*Nf1* animals had enlarged brachial plexi, several large dorsal root ganglia and enlarged trigeminal nerves (Fig. 2A, **middle** & **right**, respectively). Importantly, *Pten* dosage with *Nf1* inactivation affected enlarged dorsal root ganglia tumor multiplicity between Δ*Nf1*/Δ*Pten* and Δ*Nf1*/*Pten-het* animals. Δ*Nf1*/Δ*Pten* animals had significantly more enlarged dorsal root ganglia, compared with Δ*Nf1*/*Pten-het* animals ($P < 0.0001$, unpaired *t*-test) (Fig. 2B and Table 1). *Pten* loss contributed to enlarged dorsal root ganglion formation as seen in *Nf1-het*/Δ*Pten* and Δ*Pten* animals. The median survival age and number of enlarged dorsal root ganglia from *Nf1-het*/Δ*Pten* and Δ*Pten* animals were shown in Supplementary Figure 2 and Table 1. Both *Nf1-het*/Δ*Pten* and Δ*Pten* animals had an increased incidence of enlarged brachial plexi and trigeminal nerves (Supplementary Fig. 2 and Table 1). Enlarged peripheral nerves from *Nf1-het*/Δ*Pten* and Δ*Pten* animals were graded as low-grade PNSTs, while enlarged peripheral nerves from Δ*Nf1*/Δ*Pten* experimental animals were graded as high-grade PNSTs by histology and Ki67 staining criteria as depicted (18, 19) (Table 1). Δ*Nf1*/Δ*Pten* experimental animals had enlarged brachial plexi and trigeminal nerves at 100% occurrence ($n = 11$), while Δ*Nf1*/*Pten-het* animals had enlarged brachial plexi and trigeminal nerves at 92.3% and 69.2% occurrence ($n = 13$), respectively (Table 1). Occurrence of other peripheral nerve phenotype seen in Δ*Nf1*/Δ*Pten* experimental animals ($n = 11$) included enlarged lumbar sacral plexi (54.5%) and enlarged sciatic nerves (63.6%) (Table 1). It appears that *Pten* inactivation was required for lumbar plexi tumorigenesis, and that a dose-dependent effect exists as more tumors were found in animals with both alleles inactivated compared to animals with one allele inactivated. As for Δ*Nf1*/*Pten-het* animals ($n = 13$), occurrence of enlarged lumbar sacral plexi and sciatic nerves were seen at 15.4% and 7.7%, respectively (Table 1). The occurrence of various peripheral nerve phenotypes in other experimental and control cohorts is shown in Table 1.

Mouse model recapitulates the human disease

Importantly, Δ*Nf1*/Δ*Pten* and Δ*Nf1*/*Pten-het* experimental animals generated in the current study demonstrated various phenotypes that recapitulate the human NF1 disease (Fig. 3). These phenotypes included intercostal and paraspinal neurofibromas; and enlarged brachial and lumbar sacral plexi.

Histopathological and immunohistochemical (IHC) analyses revealed mice developed low-grade and high-grade PNSTs

Histopathological and immunohistochemical (IHC) analyses of peripheral nervous system tissues taken from both experimental cohorts demonstrated high-grade PNSTs in Δ*Nf1*/Δ*Pten* animals (Fig. 4A) compared to low-grade PNSTs seen in Δ*Nf1*/*Pten-het* animals (Fig. 4B). Enlarged peripheral nervous system tissues taken from Δ*Pten* and *Nf1-het*/Δ*Pten* animals were generally low-grade PNSTs. Importantly, enlarged peripheral nerves taken from two representative Δ*Nf1*/Δ*Pten* and Δ*Nf1*/*Pten-het* animals were positive for S100β and Olig2 staining, indicating a Schwann cell and/or precursor cell origin (Fig. 4A and 4B). These cells were also Ki67-positive at varying intensities, indicative of cell proliferation (Fig. 4A and 4B). Enlarged peripheral nerves taken from Δ*Nf1*/Δ*Pten* and Δ*Nf1*/*Pten-het* animals were both pErk1/2 positive by IHC, levels were higher than detected in normal nerves (Supplementary Fig. 3) thus confirming that the conditional inactivation of *Nf1* in Schwann cells and/or their precursor cells resulted in activated *Ras*/*Mapk*/*Erk* signaling (Fig. 4A and 4B). Enlarged peripheral nerves taken from Δ*Nf1*/Δ*Pten* animals were also pAkt positive by IHC, levels were higher than detected in normal nerves (Supplementary Fig. 3) thus confirming the conditional inactivation of *Pten* in Schwann cells and/or their precursor cells results in activated *Pi3k*/*Akt*/*mTor* signaling (Fig. 4A). Similarly, *Nf1-het*/

Δ*Pten* animals were also pAkt positive by IHC (Supplementary Fig. 3). In contrast, Δ*Nf1*/*Pten-het* animals were slightly positive for pAkt likely reflecting partial inactivation of *Pten* in Schwann cells and/or their precursor cells (Fig. 4B). Both Δ*Nf1*/Δ*Pten* and Δ*Nf1*/*Pten-het* animals were positive for pS6, a downstream effector gene and indicator for *Akt*/*mTor* activation (Fig. 4A and 4B). Interestingly, the wild-type Pten allele in Δ*Nf1*/*Pten-het* animals appeared to be intact, as peripheral nerves stained positive for Pten by immunofluorescence (Fig 4C). Semi-quantitative analysis for Ki67-positive cells was performed on representative peripheral nerves taken from control and experimental cohorts (Supplementary Fig. 4). There was no significant difference in number of Ki67-positive cells in cohorts with low-grade PNSTs (Table 1 and Supplementary Fig. 4). However, significant differences ($P < 0.01$) were seen in the number of Ki67-positive cells in Δ*Nf1*/Δ*Pten* animals with high-grade PNSTs when compared with other cohorts (Table 1 and Supplementary Fig. 4).

Microarray gene expression analysis of human peripheral nerve tumor samples

Both *PTEN* and *NF1* levels in purified Schwann cells taken from human peripheral nerve, neurofibroma and MPNST cell lines (Fig. 5A) and solid tumors (Fig. 5B) at various stages of disease were analyzed by microarray gene expression analysis. As expected in NF1 patients, *NF1* expression levels were reduced in the majority of samples tested (Fig. 5A & 5B). Although there may be a trend to reduced *PTEN* expression levels at early stages of the disease, there was a dramatic decrease in its expression level in the malignant stage of the disease (Fig. 5A & 5B).

Discussion

The present study shows that conditional inactivation of both *Nf1* and *Pten* genes in Schwann cells and/or their precursor cells results in lethality by 15-days after birth. Histopathological analyses of enlarged peripheral nerves isolated from Δ*Nf1*/Δ*Pten* animals classified tumors as high-grade PNSTs, in contrast to the low-grade PNSTs in Δ*Nf1*/*Pten-het* animals. Interestingly, *Pten* dosage augmented the peripheral nervous system phenotype in the context of *Nf1* inactivation in Schwann cells and/or their precursor cells, but peripheral nervous system phenotype was not significantly affected by *Nf1* dosage in the context of *Pten* inactivation (Fig. 1B). It has also been previously shown that *Pten* dosage in mice is essential for neurofibroma development and malignant transformation, but not in the context of *Nf1* loss in Schwann cells and/or their precursor cells (13). Gregorian *et al.* used the *mGFAP*-Cre together with conditional *Nf1* and *Pten* alleles but found no tumors. This discrepancy in phenotype could be attributed to the different Cre used, which may represent a difference in the initiating cell type or stain background effects (13). Importantly, this conditional inactivation of *Pten* and *Nf1* mouse model can accurately recapitulate the different peripheral nervous phenotypes associated with the human NF1 syndrome (Fig. 3).

Human NF1 patients' neurofibromas seem to undergo changes that result in reduced *PTEN* expression during the progression from benign neurofibromas to MPNSTs (Fig. 5A & 5B). This may also be occurring in sporadic cases of MPNSTs as previous direct comparative microarray expression analyses showed no consistent differences between NF1-associated and sporadic MPNSTs (21). Thus, we propose that loss of *PTEN* is an important step in the malignant progression of neurofibromas. This hypothesis was further strengthened when in a separate forward genetic screen for genes responsible for sporadic MPNST using the *Sleeping Beauty* transposon insertional mutagenesis system, *Nf1* and *Pten* were identified as two potential mutational driver genes in the majority of high-grade PNSTs (*manuscript in preparation*).

Δ*Nf1*/*Pten-het* animals developed low-grade PNSTs earlier compared to Δ*Nf1* control animals, indicating that *Pten* dosage is important for neurofibroma tumorigenesis in the context of *Nf1* loss in Schwann cells and/or their precursor cells. There was no statistical difference in the survival rate between Δ*Pten* and Δ*Nf1* ($P = 0.3660$, log-rank test), indicating that loss of either tumor suppressor gene can promote Schwann cell tumorigenesis. Constitutive activation of either *Ras*/*Mapk/Erk* or *Pi3k*/*Akt*/*mTor* pathways alone may not be sufficient for tumor initiation and/or progression as Δ*Nf1* and Δ*Pten* animals control animals develop a peripheral nervous system phenotype similar to one another (Table 1). When one allele of *Pten* was inactivated in the context of *Nf1* loss to allow for partial activation of the *Pi3k*/*Akt*/*mTor* pathway, we observed a significantly reduced latency in tumorigenesis when compared to animals with *Nf1* inactivated only. As Δ*Nf1*/*Pten-het* tumors retained Pten protein expression (Fig. 4C), this result suggests that *Pten* is haploinsufficient for tumor suppression in this context. Genetic events that reduce *PTEN* expression or activity are likely to be strongly selected for during MPNST progression. Thus, therapeutic agents that target *PI3K*/*AKT* signaling may be very useful for MPNST treatment or prevention strategies. Latency was further reduced and transformation augmented when both *Nf1* and *Pten* were inactivated, increasing tumor multiplicity and disease progression from low-grade to high-grade PNSTs with both *Ras*/*Mapk/Erk* and *Pi3k*/*Akt*/*mTor* pathways activated (Fig. 4A & 5C). It has been shown that the activation of the *PI3K*/*AKT* and *MAPK*/*ERK* signaling pathways may be responsible for the underlying biological aggressiveness in human pilocytic astrocytomas, a condition also found in NF1 patients (22). This could be precisely what is occurring in this novel mouse model with conditional inactivation of *Nf1* and *Pten* in Schwann cells, as evident with the rapid manifestation of high-grade PNSTs. Staining for pS6 in both Δ*Nf1*/Δ*Pten* and Δ*Nf1*/*Pten-het* peripheral nerves suggest activation of *mTor* signaling (Fig. 4A). However, hyperactivation of *mTor* signaling has also been demonstrated in $Nf1^{-/-}$ astrocytes (23).

Taken together, these results suggest that *Pten* dosage, in the context of *Nf1* loss in Schwann cells and/or their precursor cells, is essential for the progression from low-grade to high-grade PNSTs. Interestingly, both Δ*Nf1*/*Pten-het* and Δ*Nf1*/Δ*Pten* animals generated a variety of different peripheral nervous system phenotype commonly seen in human NF1 patients, with higher penetrance and phenotypic diversity seen in Δ*Nf1*/Δ*Pten* animals (Table 1). Thus, this model can be used to accurately recapitulate the human disease and to potentially rapidly test a variety of pharmaceutical compounds *in vivo*.

Supplementary Material

Refer to Web version on PubMed Central for supplementary material.

Acknowledgments

Funding provided by the National Institute of Health-NINDS-P50 N5057531 and the Margaret Harvey Schering Trust.

References

1. Boyd KP, Korf BR, Theos A. Neurofibromatosis type 1. J Am Acad Dermatol. 2009; 61:1–14. quiz 5–6. [PubMed: 19539839]
2. Friedman JM. Epidemiology of neurofibromatosis type 1. Am J Med Genet. 1999; 89:1–6. [PubMed: 10469430]
3. Rosenfeld A, Listernick R, Charrow J, Goldman S. Neurofibromatosis type 1 and high-grade tumors of the central nervous system. Childs Nerv Syst. 2010; 26:663–7. [PubMed: 19937438]

4. Maertens O, Brems H, Vandesompele J, De Raedt T, Heyns I, Rosenbaum T, et al. Comprehensive NF1 screening on cultured Schwann cells from neurofibromas. Hum Mutat. 2006; 27:1030–40. [PubMed: 16941471]
5. Serra E, Ars E, Ravella A, Sanchez A, Puig S, Rosenbaum T, et al. Somatic NF1 mutational spectrum in benign neurofibromas: mRNA splice defects are common among point mutations. Hum Genet. 2001; 108:416–29. [PubMed: 11409870]
6. Serra E, Puig S, Otero D, Gaona A, Kruyer H, Ars E, et al. Confirmation of a double-hit model for the NF1 gene in benign neurofibromas. Am J Hum Genet. 1997; 61:512–9. [PubMed: 9326316]
7. Carroll SL, Ratner N. How does the Schwann cell lineage form tumors in NF1? Glia. 2008; 56:1590–605. [PubMed: 18803326]
8. Keng VW, Villanueva A, Chiang DY, Dupuy AJ, Ryan BJ, Matise I, et al. A conditional transposon-based insertional mutagenesis screen for genes associated with mouse hepatocellular carcinoma. Nat Biotechnol. 2009; 27:264–74. [PubMed: 19234449]
9. Dupuy AJ, Rogers LM, Kim J, Nannapaneni K, Starr TK, Liu P, et al. A modified sleeping beauty transposon system that can be used to model a wide variety of human cancers in mice. Cancer Res. 2009; 69:8150–6. [PubMed: 19808965]
10. Starr TK, Allaei R, Silverstein KA, Staggs RA, Sarver AL, Bergemann TL, et al. A transposon-based genetic screen in mice identifies genes altered in colorectal cancer. Science. 2009; 323:1747–50. [PubMed: 19251594]
11. Wu J, Williams JP, Rizvi TA, Kordich JJ, Witte D, Meijer D, et al. Plexiform and dermal neurofibromas and pigmentation are caused by Nf1 loss in desert hedgehog-expressing cells. Cancer Cell. 2008; 13:105–16. [PubMed: 18242511]
12. Hollander MC, Blumenthal GM, Dennis PA. PTEN loss in the continuum of common cancers, rare syndromes and mouse models. Nat Rev Cancer. 2011; 11:289–301. [PubMed: 21430697]
13. Gregorian C, Nakashima J, Dry SM, Nghiemphu PL, Smith KB, Ao Y, et al. PTEN dosage is essential for neurofibroma development and malignant transformation. Proc Natl Acad Sci U S A. 2009; 106:19479–84. [PubMed: 19846776]
14. Zhu Y, Ghosh P, Charnay P, Burns DK, Parada LF. Neurofibromas in NF1: Schwann cell origin and role of tumor environment. Science. 2002; 296:920–2. [PubMed: 11988578]
15. Xiao A, Yin C, Yang C, Di Cristofano A, Pandolfi PP, Van Dyke T. Somatic induction of Pten loss in a preclinical astrocytoma model reveals major roles in disease progression and avenues for target discovery and validation. Cancer Res. 2005; 65:5172–80. [PubMed: 15958561]
16. Jaegle M, Ghazvini M, Mandemakers W, Piirsoo M, Driegen S, Levavasseur F, et al. The POU proteins Brn-2 and Oct-6 share important functions in Schwann cell development. Genes Dev. 2003; 17:1380–91. [PubMed: 12782656]
17. Viskochil DH. It takes two to tango: mast cell and Schwann cell interactions in neurofibromas. J Clin Invest. 2003; 112:1791–3. [PubMed: 14679174]
18. Stemmer-Rachamimov AO, Louis DN, Nielsen GP, Antonescu CR, Borowsky AD, Bronson RT, et al. Comparative pathology of nerve sheath tumors in mouse models and humans. Cancer Res. 2004; 64:3718–24. [PubMed: 15150133]
19. Weiss WA, Israel M, Cobbs C, Holland E, James CD, Louis DN, et al. Neuropathology of genetically engineered mice: consensus report and recommendations from an international forum. Oncogene. 2002; 21:7453–63. [PubMed: 12386807]
20. Hummel TR, Jessen WJ, Miller SJ, Kluwe L, Mautner VF, Wallace MR, et al. Gene expression analysis identifies potential biomarkers of neurofibromatosis type 1 including adrenomedullin. Clin Cancer Res. 2010; 16:5048–57. [PubMed: 20739432]
21. Miller SJ, Rangwala F, Williams J, Ackerman P, Kong S, Jegga AG, et al. Large-scale molecular comparison of human schwann cells to malignant peripheral nerve sheath tumor cell lines and tissues. Cancer Res. 2006; 66:2584–91. [PubMed: 16510576]
22. Rodriguez EF, Scheithauer BW, Giannini C, Rynearson A, Cen L, Hoesley B, et al. PI3K/AKT pathway alterations are associated with clinically aggressive and histologically anaplastic subsets of pilocytic astrocytoma. Acta Neuropathol. 2011; 121:407–20. [PubMed: 21113787]

23. Dasgupta B, Yi Y, Chen DY, Weber JD, Gutmann DH. Proteomic analysis reveals hyperactivation of the mammalian target of rapamycin pathway in neurofibromatosis 1-associated human and mouse brain tumors. Cancer Res. 2005; 65:2755–60. [PubMed: 15805275]

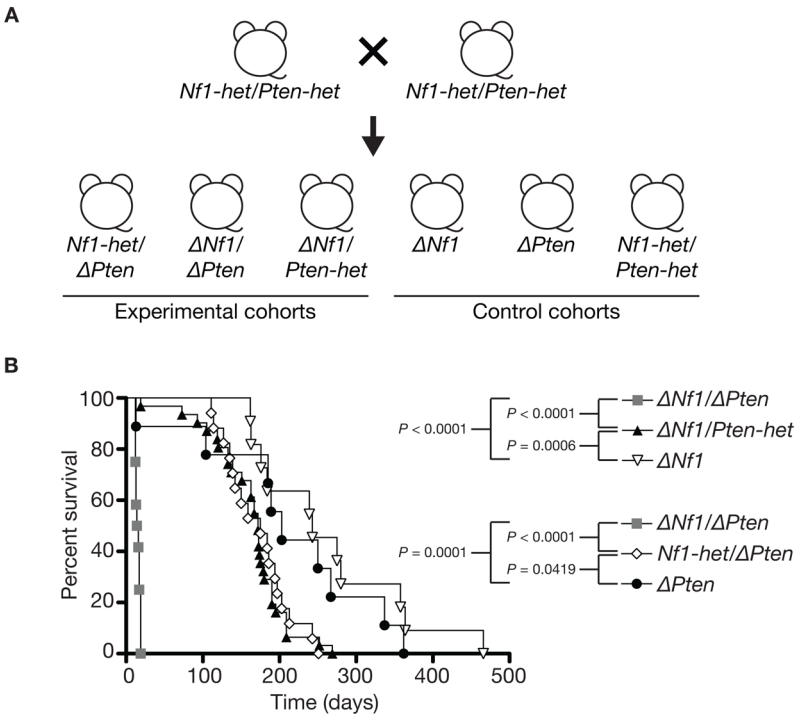

Figure 1.

Establishing a novel peripheral nerve tumor progression mouse model. (**A**) Breeding strategy for generating experimental and control animals. Transgenic mice each carrying a single transgene was interbred to obtain doubly transgenic mice. Doubly transgenic mice were then interbred with remaining transgene to obtain triple transgenic *Dhh*-Cre; $Nf1^{flox/+}$; $Pten^{flox/+}$ mice (*Nf1-het*/*Pten-het*). Finally, triple transgenic mice were interbred to obtain the experimental and control cohorts required. *Dhh*-Cre; $Nf1^{flox/+}$; $Pten^{flox/flox}$ (*Nf1-het*/Δ*Pten*), *Dhh*-Cre; $Nf1^{flox/flox}$; $Pten^{flox/flox}$ (Δ*Nf1*/Δ*Pten*) and *Dhh*-Cre; $Nf1^{flox/flox}$; $Pten^{flox/+}$ (Δ*Nf1*/*Pten-het*) experimental cohorts. *Dhh*-Cre; $Nf1^{flox/flox}$ (Δ*Nf1*), *Dhh*-Cre; $Pten^{flox/flox}$ (Δ*Pten*) and *Nf1-het*/*Pten-het* control cohorts. (**B**) Kaplan-Meier survival curves of various experimental and control cohorts generated using the GraphPad Prism software. *Pten* dosage augmented the peripheral nervous system phenotype in the context of *Nf1* inactivation in Schwann cell and/or their precursor cells. *P*, log-rank test.

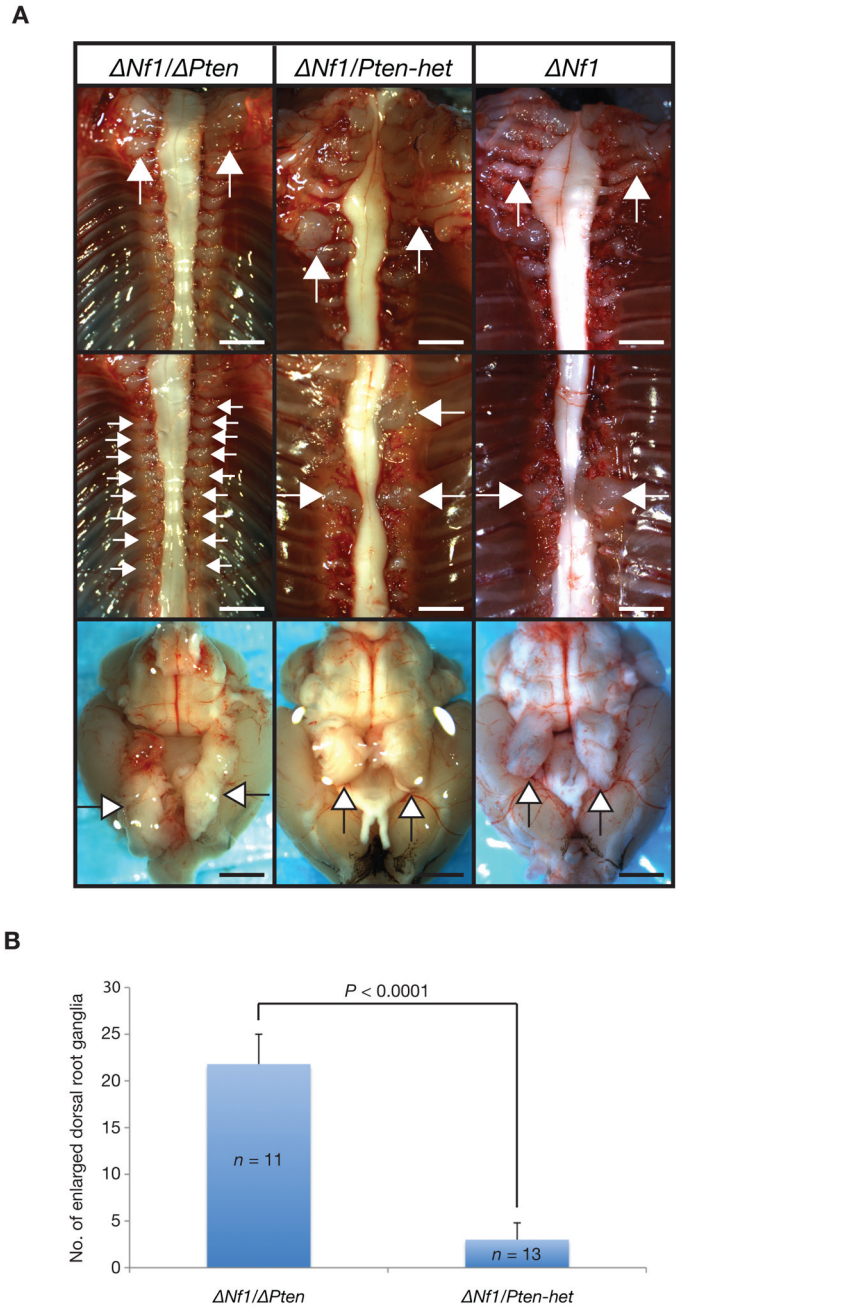

Figure 2.

Pten dosage with *Nf1* inactivation affected enlarged dorsal root ganglia tumor multiplicity. (**A**) Left, representative of an early onset peripheral nervous system phenotype observed in a 16-day *Dhh*-Cre; $Nf1^{flox/flox}$; $Pten^{flox/flox}$ (Δ*Nf1*/Δ*Pten*) experimental mouse. Enlarged brachial plexus, majority of dorsal root ganglia were enlarged and enlarged trigeminal nerves. Middle, representative of a late onset peripheral nervous system phenotype observed in a 163-day *Dhh*-Cre; $Nf1^{flox/flox}$; $Pten^{flox/+}$ (Δ*Nf1*/*Pten-het*) experimental mouse. Enlarged brachial plexus, several enlarged dorsal root ganglia and enlarged trigeminal nerves. Right, representative of a late onset peripheral nervous system phenotype observed in a 184-day *Dhh*-Cre; $Nf1^{flox/flox}$ (Δ*Nf1*) control mouse. Enlarged brachial plexus, several enlarged dorsal root ganglia and enlarged trigeminal nerves. Top panels, brachial plexi; middle

panels, dorsal root ganglia; bottom panels, brain with trigeminal nerves; arrows indicate peripheral nervous system phenotype; scale bars, 2 mm. (**B**) Statistically significant differences in the number of enlarged dorsal root ganglia isolated from each experimental cohort when animals became moribund (median survival ages for Δ*Nf1*/Δ*Pten* and Δ*Nf1*/*Pten-het* were 15- and 163-days, respectively). Mean ± SD; *P*, unpaired *t*-test; *n*, number of mice evaluated in each cohort.

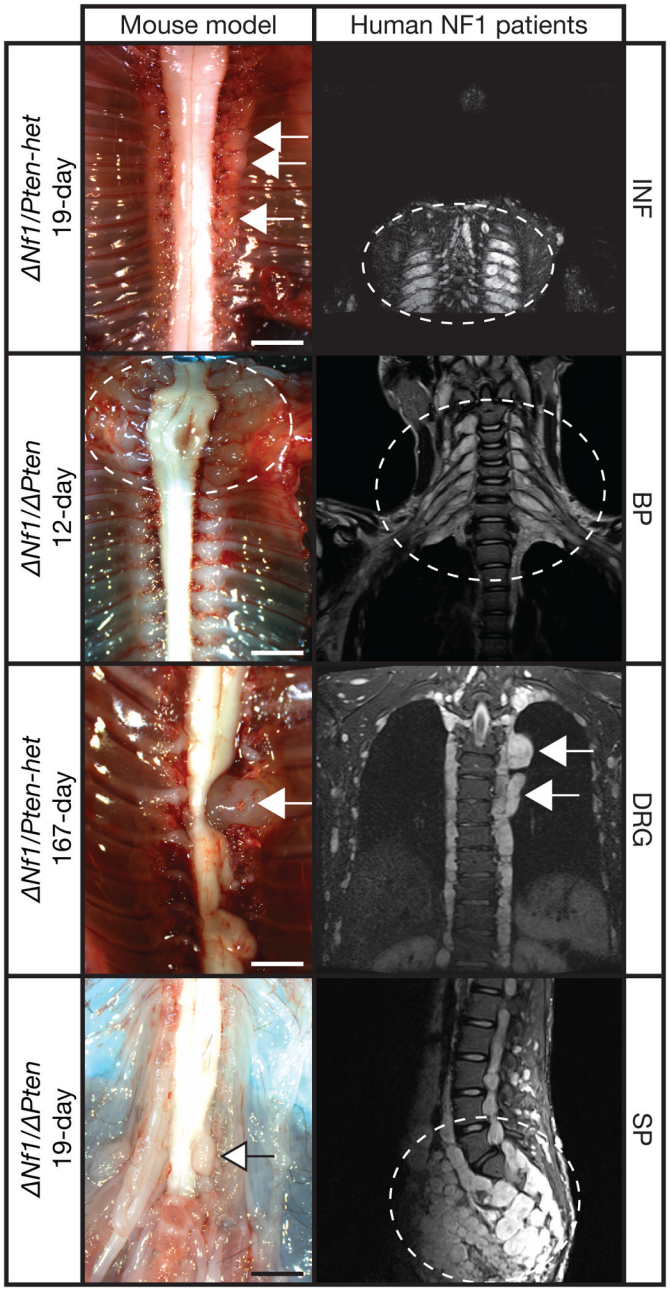

Figure 3.

Recapitulating the human NF1 condition using mouse models. The various peripheral nervous system phenotype demonstrated by *Dhh*-Cre; $Nf1^{flox/flox}$; $Pten^{flox/flox}$ (Δ*Nf1*/Δ*Pten*) and *Dhh*-Cre; $Nf1^{flox/flox}$; $Pten^{flox/+}$ (Δ*Nf1*/*Pten-het*) experimental animals at various ages indicated (**left**) clearly recapitulates the human NF1 disease as depicted in the MRI images (**right**). INF, intercostal neurofibromas; BP, enlarged brachial plexi; DRG, enlarged dorsal root ganglia; SP, enlarged lumbar sacral plexi. Arrows and dashed lines indicate peripheral nervous system phenotype. Scale bars, 2 mm.

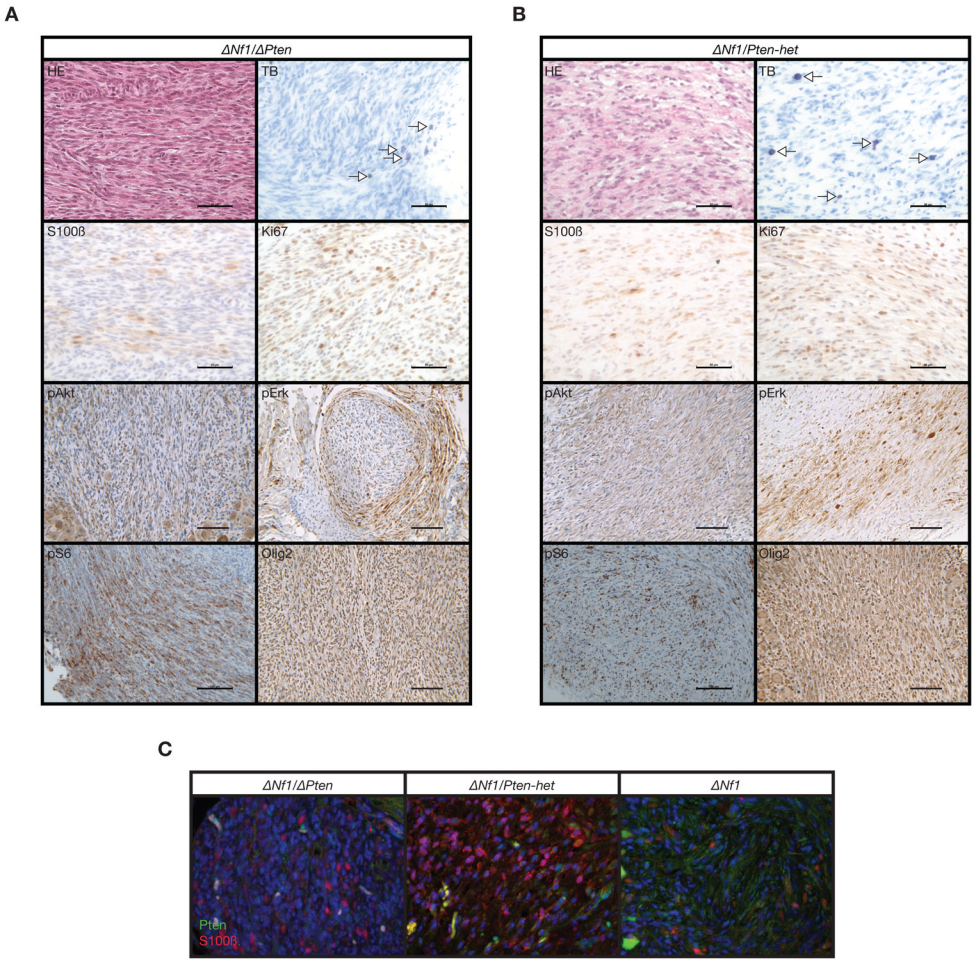

Figure 4.

Histological analyses of peripheral nervous system phenotype. Standard hematoxylin-eosin staining (HE) and toluidine blue (TB) staining were performed on all peripheral nervous system tissue sections (**A** & **B**). Immunohistochemical (IHC) staining using antibodies against the proliferative marker (Ki67), Schwann cell/oligodendrocyte lineage marker (S100β and Olig2), activated *Ras/Mapk/Erk* signaling by phospho-Erk1/2 (pErk), activated *Pi3k/Akt* signaling by phospho-Akt detection and activated *mTor* signaling by phospho-S6 (pS6) (**A** & **B**). Negative controls, sections incubated without the primary antibody gave no significant signal above background. (**A**) Representative HE, TB and IHC analyses of enlarged peripheral nerve from a representative *Dhh*-Cre; $Nf1^{floxflox}$; $Pten^{flox/flox}$ (Δ*Nf1*/Δ*Pten*) experimental mouse. Scale bars, 50 μm. (**B**) Representative HE, TB and IHC analyses of enlarged peripheral nerve from a representative *Dhh*-Cre; $Nf1^{floxflox}$; $Pten^{flox/+}$ (Δ*Nf1*/*Pten-het*) experimental mouse. Scale bars, 50 μm. Representative IHC staining showing elevated pErk levels in peripheral nerves taken from Δ*Nf1*/Δ*Pten* and Δ*Nf1*/*Pten-het* animals likely as a result of *Nf1* inactivation. Scale bar, 100 μm. Representative IHC staining showing elevated pAkt levels in peripheral nerve from a Δ*Nf1*/Δ*Pten* animal but only slightly elevated levels in a Δ*Nf1*/*Pten-het* animal likely as a result of *Pten* gene dosage response. Scale bar, 100 μm. Representative IHC staining showing elevated pS6 levels in peripheral nerve from a Δ*Nf1*/Δ*Pten* animal but only slightly elevated levels in a Δ*Nf1*/*Pten-het* animal. Scale bar, 100 μm. Arrows in TB-stained panels indicate mast cells (**A** & **B**). (**C**) Representative fluorescent images showing increase in Pten protein levels as gene

dosage increases in Δ*Nf1*/Δ*Pten*, Δ*Nf1*/*Pten-het* and *Dhh*-Cre; $Nf1^{floxflox}$ (Δ*Nf1*) animals. Peripheral nerves were co-stained with an anti-S100β (red channel) to identify Schwann cells, DAPI (blue channel) to identify nuclei and anti-Pten (green channel) to detect Pten protein status.

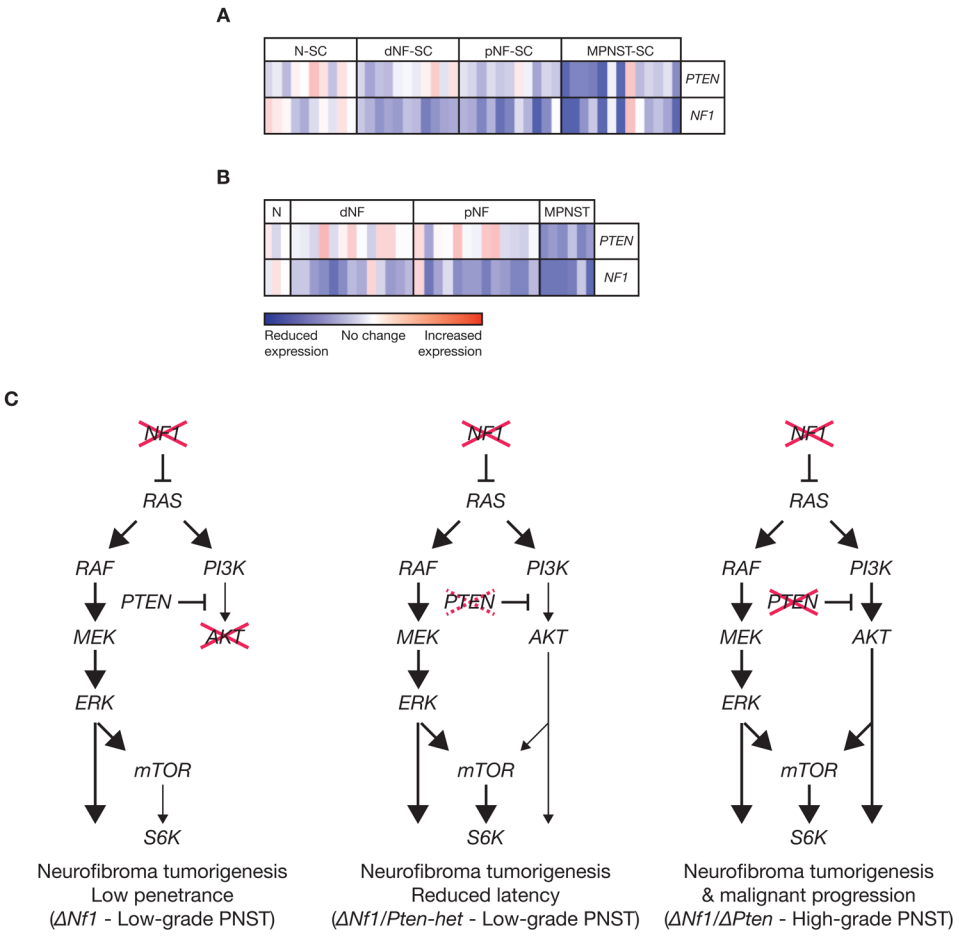

Figure 5.

Expression microarray analysis of *PTEN* and *NF1* in human peripheral nerve tumors. (**A**) Purified human Schwann cells from normal sciatic nerve (NH-SC), dermal neurofibroma cell lines (dNF-SC), plexiform neurofibroma cell lines (pNF-SC) and malignant peripheral nerve sheath cell lines (MPNST-SC). (**B**) Normal human sciatic nerve tissues (N) and solid tumors from dermal neurofibromas (dNF), plexiform neurofibromas (pNF) and malignant peripheral nerve sheath tumors (MPNST). As expected, there was a reduction in *NF1* expression levels from all stages of the disease. As the disease progressed from a benign to malignant form, decrease in *PTEN* expression was observed. Red, increase in red intensity as expression increases; Blue, increase in blue intensity as expression decreases. (**C**) Conditional inactivation of *Nf1* in Schwann cells and/or their precursor cells resulted in low-grade PNST tumorigenesis at low penetrance (**left**). However, partial conditional inactivation of *Pten* in the context of *Nf1* loss in Schwann cells and/or their precursor cells resulted in reduced latency of low-grade PNST tumorigenesis when compared to mice with *Nf1* conditional inactivation only. Genetic events that reduce *PTEN* expression or activity are likely to be strongly selected for during MPNST progression (**middle**). In contrast, conditional inactivation of both *Pten* and *Nf1* in Schwann cells and/or their precursor cells resulted in high-grade PNST initiation and/or progression due to the upregulation of both *Ras/Mapk/Erk* and *Pi3k/Akt/mTor* signaling pathways (**right**). *Dhh*-Cre; $Nf1^{flox/flox}$ (Δ*Nf1*), *Dhh*-Cre; $Nf1^{flox/flox}$; $Pten^{flox/+}$ (Δ*Nf1*/*Pten-het*) and *Dhh*-Cre; $Nf1^{flox/flox}$; $Pten^{flox/flox}$ (Δ*Nf1*/Δ*Pten*) animals.

Table 1

Occurrence of different peripheral nervous system phenotype in various experimental and control cohorts

Genotype	*N*	Median survival age (days)	*n*	Enlarged DRG (mean ± SD)	Tumor grade	BP	TN	SN	LP
Nf1$^{f/f}$; *Pten*$^{f/f}$	12	15	11	21.8 ± 3.2	High	100%	100%	64%	55%
Nf1$^{f/f}$; *Pten*$^{f/+}$	31	172	13	3.0 ± 1.8	Low	92%	69%	8%	15%
Nf1$^{f/f}$	11	243	5	3.0 ± 1.0	Low	100%	60%	60%	0%
Nf1$^{f/+}$; *Pten*$^{f/f}$	17	175	14	6.5 ± 4.0	Low	100%	100%	100%	7%
Pten$^{f/f}$	9	203	7	7.1 ± 4.5	Low	100%	86%	71%	14%

All mice were transgenic for *Dhh*-Cre. *f/f, flox/flox; f/+, flox/+; N,* total number of mice in each cohort; Median, median survival age; *n,* number of mice examined for the occurrence of various peripheral nervous system phenotype; DRG, number of enlarged dorsal root ganglia isolated (mean ± standard deviation); Grade, tumor grade was determined by histological evaluation as described in the Materials and Methods. High, high-grade PNST; Low, low-grade PNST. Percentage of animals in each cohort that displayed the following peripheral nervous system phenotype: BP, enlarged brachial plexi; TN, enlarged trigeminal nerves; SN, enlarged sciatic nerves; LP, enlarged sacral plexi.